Topological elastic interface states in hyperuniform pillared metabeams

Runcheng Cai, Yan Pennec, Laurent Carpentier, Yabin Jin, Timon Rabczuk, Xiaoying Zhuang, Bahram Djafari-Rouhani

APL Materials

RESEARCH ARTICLE | JANUARY 23 2024

Topological elastic interface states in hyperuniform pillared metabeams

Special Collection: New Frontiers in Acoustic and Elastic Metamaterials and Metasurfaces

Runcheng Cai ; Yan Pennec ; Laurent Carpentier; Yabin Jin ; Timon Rabczuk ; Xiaoying Zhuang ; Bahram Djafari-Rouhani

APL Mater. 12, 011121 (2024)
https://doi.org/10.1063/5.0184699

APL Materials ARTICLE pubs.aip.org/aip/apm

Topological elastic interface states in hyperuniform pillared metabeams

Cite as: APL Mater. 12, 011121 (2024); doi: 10.1063/5.0184699
Submitted: 26 October 2023 • Accepted: 28 December 2023 •
Published Online: 23 January 2024

Runcheng Cai,[1,2] Yan Pennec,[2] Laurent Carpentier,[2] Yabin Jin,[3,a)] Timon Rabczuk,[4] Xiaoying Zhuang,[1,5,a)] and Bahram Djafari-Rouhani[2,a)]

AFFILIATIONS

[1] Department of Geotechnical Engineering, College of Civil Engineering, Tongji University, 200092 Shanghai, China
[2] Institut d'Electronique, de Microélectonique et de Nanotechnologie, UMR CNRS 8520, Département de Physique, Université de Lille, 59650 Villeneuve d'Ascq, France
[3] School of Aerospace Engineering and Applied Mechanics, Tongji University, 200092 Shanghai, China
[4] Institute of Structural Mechanics, Bauhaus-Universität Weimar, Weimar D-99423, Germany
[5] Institute of Photonics, Department of Mathematics and Physics, Leibniz University Hannover, Hannover, Germany

Note: This paper is part of the Special Topic on New Frontiers in Acoustic and Elastic Metamaterials and Metasurfaces.
[a)] **Authors to whom correspondence should be addressed:** 083623jinyabin@tongji.edu.cn; xiaoyingzhuang@tongji.edu.cn; and bahram.djafari-rouhani@univ-lille.fr

ABSTRACT

Topological states have been receiving a great deal of interest in various wave problems, such as photonic, acoustic, and elastic waves. However, few studies of topological elastic waves in non-periodic systems have been reported. Recently, hyperuniform systems suppressing long-range order while partly maintaining short-range order have provided new opportunities to control waves. In this work, we study the elastic topological interface states appearing between two Su–Schrieffer–Heeger (SSH)-like pillared metabeams where each metabeam, is constituted by a mirror symmetric hyperuniform structure. The SSH-like model is constructed by combining two hyperuniform metabeams with inverted configurations. We demonstrate that this structure could open new bandgaps at low frequencies, of which some are nontrivial and can support topological interface modes. We further show that the number of low-frequency bandgaps supporting the topological modes increases with the level of randomness, hence providing a high number of interface modes in the same structure. The robustness of the topological interface states against random perturbations in the pillars' positions is further verified. Our work offers a reliable platform for studying topological properties and hyperuniform metamaterials and designing wave control devices for low-frequency wave attenuation and robust energy localization.

I. INTRODUCTION

Artificially structured materials such as phononic crystals[1–4] and acoustic metamaterials,[5–7] which consist of periodic or non-periodic arranged units, have attracted much interest owing to their unusual properties in terms of wave attenuation, energy harvesting, waveguiding, and sensing. In recent years, topological physics, as an emerging field, has provided anomalous wave properties and is being used to design novel artificially structured materials to manipulate acoustic and elastic waves robustly.[8–11] The key feature of a topological system is the existence of topologically protected states at the interface between two systems with distinct topological invariants, whose existence is robust against defects and impurities and makes them immune to backscattering in two-dimensional systems. In a one-dimensional (1D) system, the topological invariant is expressed by the Zak phase, which is a special kind of Berry phase associated with each 1D bulk band.[12] Then, various topological effects, such as topological interface states,[13,14] topological exceptional points,[15] and robust Fano resonances,[16,17] have been investigated.

One of the most widely used models to predict and investigate the topological states in one-dimensional systems is the Su–Schrieffer–Heeger (SSH) model.[18] This model describes a discrete system with a dimerized unit cell, where the trivial or nontrivial character is defined by the fact that the ratio between the hopping integrals of intracell and intercell atoms is less or greater than one. Accordingly, the existence of a topological edge (or surface) mode localized at the free boundary of the system is demonstrated. Based on the original SSH model, many effective SSH-like models have been proposed in photonics as well as in acoustic and mechanical continuous systems.[12,19–22] The SSH-like models are constructed by associating two subsystems with different topological phases, usually accompanied by symmetry inversion of the modes at the band edges.[17,22] The topological edge states appear now at the interface between the two topological phases instead of at the open boundary of the subsystems. The bulk-boundary correspondence for the SSH-like models relates the difference between the topological phases of the two subsystems and the topological interface mode of the combined system. To predict the existence of the topological interface modes, the Zak phases of the 1D systems can be determined by the symmetry of the band-edge states of the subsystems.[12] If the Zak phases of the common bandgaps for the two subsystems are different, the bandgaps are nontrivial, and a topological interface mode is expected in the nontrivial bandgap. In practice, these interface modes can be studied in two ways: either by associating two semi-infinite (or sufficiently long finite) subsystems or by considering a periodic structure in which the unit cell is a large supercell made up of the association of two finite subsystems. In both cases, they are localized around the interface and decay when going far from the interface. Both approaches are used in the following study. Note that in the periodic case, the interface modes appear ideally as flat (dispersionless) branches among the dispersion curves; however, the degree of their flatness is related to the size of the supercell that avoids the interaction between the topological interfaces in two neighboring unit cells.

Recently, the topological states in non-Hermitian systems have been studied with the development of non-Hermitian physics.[23–25] Fan *et al.* presented an SSH-like elastic metamaterial and showed that topological edge states can be obtained when uneven absorptive dampings are applied to the unit cell, even if the hopping strengths are identical.[26] The interplay between non-Hermiticity and topological systems will lead to topological physics beyond the Bloch band theory and bulk-boundary correspondence, in which the non-Hermitian skin effect appears and has drawn lots of attention.[27–29] However, most of the topological states are studied in periodic systems.

Lately, the concept of hyperuniform disorder has been introduced to metamaterials, which were first used to estimate point patterns according to their local density fluctuations[30–33] and exhibit the properties of liquids (amorphous) and crystals (periodic) simultaneously.[34] Hyperuniform systems can suppress large-scale density fluctuations, but they are statistically isotropic and lack long-range order.[32,35] Hyperuniform systems represent the low-k limit of stealth systems, which can completely suppress the scattering of incident waves for a set of wave vectors; namely, the hyperuniform systems are transparent in the long-wavelength limit.[36–38] Consequently, periodic systems belong to the hyperuniform systems, which can suppress the scattering for all wavelengths except those associated with Bragg scattering. The hyperuniform metamaterials were found to possess large isotropic photonic/phononic bandgaps[39,40] and have been efficiently used for free-form waveguides,[41] high-Q cavities,[42] integrated waveguide polarizers,[43] vibration concentration,[44] and graded effective index materials.[45] Recently, the topological properties of hyperuniform systems have been studied. Mitchell *et al.* constructed amorphous Chern insulators from arbitrary underlying structures, including hyperuniform systems, where local decorations control the topology of the vibrational spectrum.[46] Kuznetsova *et al.* experimentally presented the topological interface modes between two SSH-like one-dimensional hyperuniform acoustic systems with different geometrical representations.[34] However, few explorations of hyperuniform systems for topological elastic waves have been reported, especially owing to the fact that elastic structures such as beams support multiple modes.

In this work, we present the topological interface modes between two SSH-like hyperuniform pillared metabeams with different Zak phases. We first state the model of the pillared metabeam and illustrate the hyperuniform distribution with the structure factors. Then we calculate the band structures of hyperuniform pillared metabeams by the supercell method and obtain the Zak phases of bandgaps via the symmetry of band-edge states. Furthermore, we construct the SSH-like model by combining the two hyperuniform metabeams, which have inversed left half and right half, and demonstrate the topological interface modes by band structures, eigenmodes of finite metabeams, and transmissions. We emphasize the increase in the number of bandgaps at low frequencies and associated interface modes when increasing the level of disorder in the hyperuniform supercell. Finally, the robustness of the topological interface modes is checked by introducing perturbations in the pillars' positions. Our study connects hyperuniform systems and topological elastic waves and could open new pathways to applications, such as broadband wave attenuation, sensing, and robust energy localization. The outline of the paper is as follows: After the introduction in Sec. I, the model of the metabeam and hyperuniform distribution are presented in Sec. II; in Sec. III, the Zak phases of the hyperuniform metabeam are obtained, and the topological interface states of the SSH-like model are demonstrated and discussed, in particular, as a function of the disorder level. Section IV is devoted to the conclusions and remarks.

II. MODEL OF THE METABEAM WITH HYPERUNIFORM DISTRIBUTION OF PILLARS

A hyperuniform pillared metabeam is constructed by arranging the pillars symmetrically on the upper and lower surfaces of the host beam, as shown in Fig. 1(a). The number N of pillars is 20, and the positions of pillars follow the hyperuniform distributions. The pillar distribution has mirror symmetry, with the mirror plane indicated by the orange dashed line in Fig. 1(a). The left and right halves, each with ten pillars, are, respectively, called S and S*. To construct an SSH-like model, we invert the left and right halves and get the counterpart S*S. Then we put the supercells SS* and S*S together and obtain the combined supercell SS*S*S, as shown in Fig. 1(b). The topological interface modes will occur at the interface of SS* and S*S, as marked by the vertical black dotted line in Fig. 1(b).

The host beam and pillars are made of aluminum, with a density of 2730 kg/m^3, Young's modulus of 77.6 GPa, and Poisson's ratio

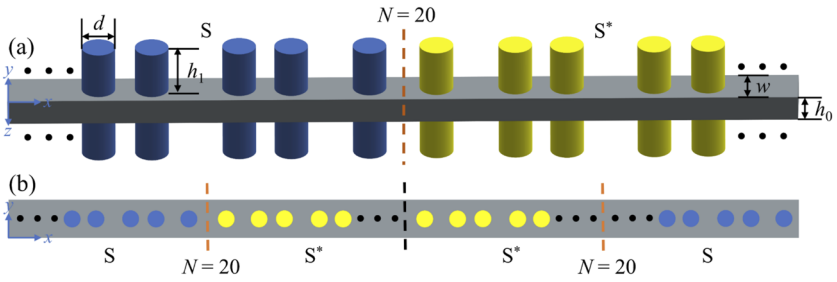

FIG. 1. (a) Schematic illustration of the hyperuniform pillared metabeam with mirror symmetry. The orange dashed line represents the mirror plane. The left and right parts of the mirror plane are, respectively, called S and S*. (b) Schematic illustration of the combined supercell SS*S*S. The black dashed line indicates the interface.

of 0.35. The diameter d and height h_1 of the pillar are 1 and 1.35 cm, respectively. The width w and height h_0 of the host beam are 2 and 1 cm, respectively.

Consider a 1D distribution of $N = 20$ identical pillars located at positions x_j. The structure factor $S(q)$ of this point pattern is defined in Fourier space and reads[36,47]

$$S(q) = \frac{1}{N}\left|\sum_{j=1}^{N} e^{iqx_j}\right|^2, \tag{1}$$

where $q = 2\pi n/L$ is the reciprocal lattice vector component, and n is the positive or negative integer, or zero. $L = Na$ is the total size, with the a lattice constant of the periodic case being 2 cm in our geometry.

Hyperuniform point patterns are characterized by the vanishing structure factor $S(q)$ in the long-wavelength limit, namely, vanishing around the origin.[35–37] In particular, this can be expressed as $S(q \le q_c) = 0$, with q_c as the cut-off reciprocal vector defining the bound of constrained reciprocal vectors. The stealthiness parameter χ can be introduced to characterize the level of disorder in the hyperuniform structure, which represents the ratio of the number of constrained degrees of freedom relative to the total number of degrees of freedom.[35,48] In our studied 1D model, the stealthiness parameter χ writes[47]

$$\chi = \frac{q_c L}{2\pi N}. \tag{2}$$

Note that the stealthiness parameter χ is bounded in the interval [0, 1]. The larger the stealthiness parameter χ is, the more ordered the structure is, namely, the closer it is to a periodic structure.

To get the target hyperuniform point patterns with different stealthiness parameters χ, we use the collective coordinate optimization technique to find the point positions x_j.[32,35,48] Briefly, the collective coordinate $C(q)$ in the 1D model is defined as

$$C(q) = \sum_{j=1}^{N-1}\sum_{l=j+1}^{N} \cos\left[q(x_j - x_l)\right]. \tag{3}$$

The structure factor $S(q)$ for a configuration can be expressed in terms of $C(q)$,

$$S(q) = 1 + \frac{2}{N}C(q). \tag{4}$$

Therefore, the collective coordinate $C(q)$ has the minimum value of $-N/2$. For a stealthiness parameter χ, the corresponding point positions x_j can be obtained by making the collective coordinate $C(q)$ in the constrained region $q \le q_c$ reach the minimum value. We utilize an optimization program to deal with this, which starts with a random distribution. In addition, only the points in the left half or the right half need to be optimized due to the mirror symmetry in our model. To avoid the overlap of adjacent pillars, we generate many samples and choose the distributions that meet the non-overlapping conditions. In addition, the target hyperuniform point patterns can also be designed by simultaneously minimizing the summation of the structure factor and the standard deviation function.[47]

The generated point positions and corresponding structure factors for periodic and one realization of $\chi = 0.4$, $\chi = 0.2$, and random distributions are shown in Fig. 2. The specific positions of the hyperuniform distributions can be found in the supplementary material, Sec. I. For periodic distribution with the periodicity of a shown in Fig. 2(a), the structure factor map presents the Bragg peaks at $q = 2\pi n/a$. For the wavelength out of the Bragg peaks, the structure factor is 0. This means that a periodic distribution of scatterers can suppress scattering for all wavelengths (namely, waves can propagate almost without scattering) except those associated with Bragg scattering.[36] The Bragg bandgap will occur around the wavelength of $2\pi n/a$ due to the Bragg scattering. For the hyperuniform distribution with $\chi = 0.4$ shown in Fig. 2(b), only the structure factor around $q = 0.5$ deviates from zero compared to the periodic case. Moreover, the structure factor shows peaks at wavelengths corresponding to the Bragg scattering, which means that the system presents some hints of periodicity. This implies that the hyperuniform system keeps part of the bandgap property of the periodic structure (while the transparency range decreases). For the hyperuniform distribution with $\chi = 0.2$ shown in Fig. 2(c), the system becomes more disordered, and the structure factor deviates more from zero, representing the more and stronger scattering effects from the scatters. As soon as the distribution becomes fully random, as shown in Fig. 2(d), there is no wavelength with a zero structure factor, and random scattering is produced.

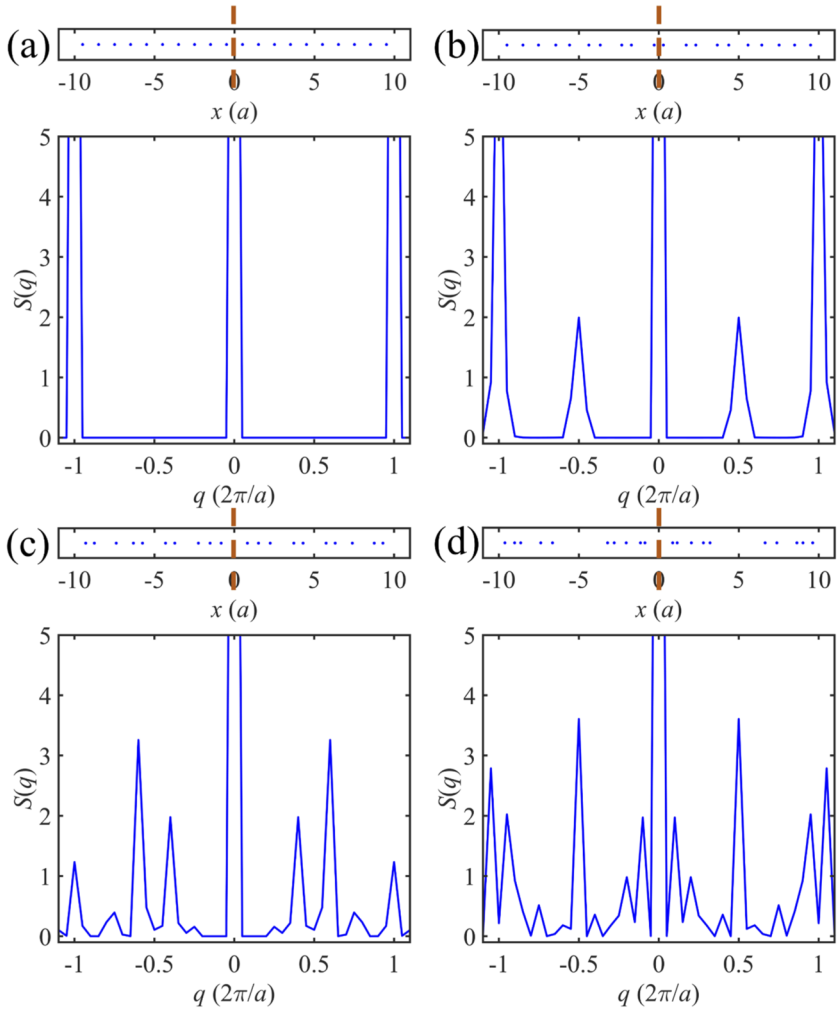

FIG. 2. Representation of the point positions (upper panels) and structure factors (lower panels) for (a) periodic, (b) $\chi = 0.4$, (c) $\chi = 0.2$, and (d) random distributions of 20 points with mirror symmetry. The orange dashed lines in the upper panels indicate the mirror planes.

III. TOPOLOGICAL STATES IN HYPERUNIFORM METABEAM

A. Periodic metabeam

We start with the properties of periodic pillared metabeams. It is worth noting that the waves propagating in the metabeam can be characterized by their symmetries and divided into four types. Indeed, the considered metabeam has two symmetry planes, *xOy* and *xOz*. Consequently, the waves propagating in the beam can be classified into four independent categories according to their symmetric or antisymmetric character with respect to the two symmetry planes. They are usually named flexural, symmetric shear, antisymmetric shear, and longitudinal modes. In this work, we focus on antisymmetric shear waves to illustrate disorder-induced multiple gaps and several topological interface states. However, the results for all four modes are presented in the supplementary material, Sec. II.

Band structures of the antisymmetric shear modes of the periodic case are shown in Fig. 3, where the first bandgap is highlighted by dark gray. The pillars have bending resonance at 31.4 kHz under antisymmetric shear wave excitation, which induces this hybrid resonant bandgap with the avoiding crossing effect. In the following study, we focus on the first hybrid resonant bandgap and study the novel effects associated with the hyperuniform structure.

B. Hyperuniform metabeam with $\chi = 0.4$

In this and the following sections, we regard the hyperuniform pillared metabeam SS* (or S*S) as a supercell and calculate the band structures of the corresponding periodic systems, which is a common approach in the study of hyperuniform structures.[40,44] First, we investigate the properties of a hyperuniform pillared metabeam with $\chi = 0.4$. Pillar positions for the hyperuniform supercell SS* and its

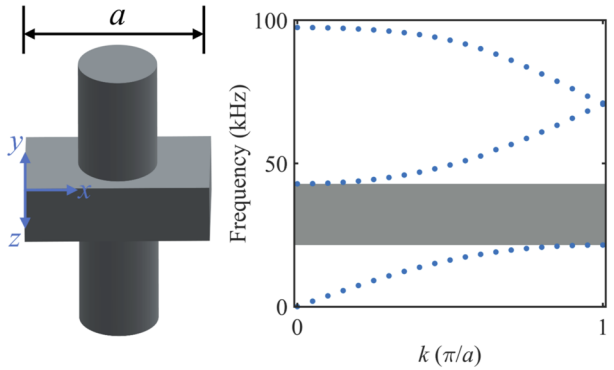

FIG. 3. Band structures of the antisymmetric shear modes in the periodic case. The dark gray region represents the locally resonant bandgap.

SSH-like counterpart S*S are shown in Figs. 4(a) and 4(b), respectively. It is worth noting that the SS* and S*S are both hyperuniform structures with the same structure factors due to the mirror symmetry. We first present the band structure of the metabeam with the supercell of 20 unit cells in the periodic case in Fig. 4(c). For the traditional discrete SSH model, the Hamiltonian or equivalent dynamical matrix can be easily written and investigated analytically by using the intracell and intercell hopping amplitudes. However, in the case of continuous systems such as our metabeams, the dynamical matrix cannot be expressed by a finite matrix Hamiltonian, and numerical methods become necessary to calculate the eigenfrequencies and eigenmodes. At best, in periodic structures with simple unit cells, the dispersion curves can be approximately reproduced by using fitting parameters for the hopping integrals, but in a disordered system, these interactions become dependent on the distances between the pillars and are most likely non-local. In Fig. 4(c), one can see that the bands fold compared to those in Fig. 3, and a hybrid bandgap appears as indicated by the dark gray region as expected, which we call the main bandgap. The band structures of the metabeams with the supercell SS* or S*S in the hyperuniform case are exactly the same, as shown in Fig. 4(d). It is noticed that new bandgaps appear for the hyperuniform metabeam compared to Fig. 4(c), which originate from the multiple scattering caused by the disordered hyperuniform distribution of pillars in the supercell. In addition, the lower boundary of the main bandgap shifts upward,

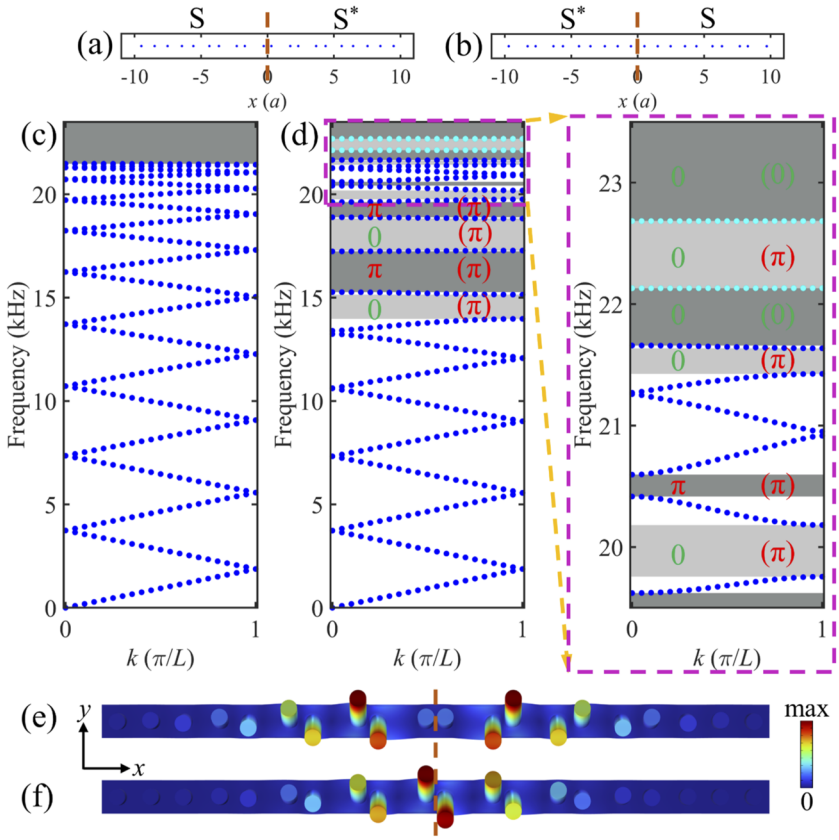

FIG. 4. Pillar positions for $\chi = 0.4$ hyperuniform supercell SS* (a) and its SSH-like counterpart S*S (b). The orange dashed lines indicate the mirror planes separating S and S*. (c) Band structures of the metabeam with the supercell of 20 unit cells in the periodic case. (d) Band structures of the metabeam with the supercells SS* (a) and S*S (b) in the hyperuniform case. The enlarged view of the high-frequency range is given in the magenta dashed box. The left and right values represent the Zak phases of bandgaps in the metabeam SS* (a) and S*S (b), respectively. The light and dark gray regions represent the nontrivial and trivial bandgaps, respectively. The modes of the lower and higher cyan bands at $k = 0$ in panel (d) are, respectively, given in (e) and (f).

and the bands near the main bandgap (namely, around the 20th band) become separated and flat. As a matter of illustration, we show in Figs. 4(e) and 4(f) the total displacement fields for the lower and upper cyan branches at $k = 0$, which appear as localized modes near the mirror plane in the considered supercell. Note that for better visualization, the displacement fields in Fig. 4 and the following are shown only in the upper half of the metabeam. Such localized modes near the main bandgap are a significant characteristic of hyperuniform systems.[38]

To explore the topological properties of hyperuniform metabeams, we calculate the Zak phase of the bandgaps. Thanks to the mirror symmetry of the supercell, the symmetry of band-edge states can be used to calculate the values of the Zak phase.[12] The band-edge states have either even or odd symmetry with respect to the mirror planes indicated by the orange dashed lines. For instance, the modes shown in Figs. 4(e) and 4(f) are of even and odd symmetry, respectively. If the two band-edge states of a band have the same symmetry, the Zak phase of this band is zero. Otherwise, the Zak phase is π. The Zak phase of a bandgap can be determined by the summation of the Zak phases of bands below this bandgap.[49] The values of Zak phases of bandgaps for hyperuniform metabeam SS* and S*S are labeled on the left and right in Fig. 4(d), respectively. When we move to the association of the metabeams SS* and S*S, the common bandgap can be considered nontrivial if the Zak phases of both metabeams are different; otherwise, it is trivial. According to the bulk-boundary correspondence, topological interface states localized between the metabeams SS* and S*S can appear within the nontrivial bandgaps when we combine the two metabeams together. The nontrivial and trivial bandgaps are indicated by the light and dark gray regions, respectively. It is found that multiple nontrivial bandgaps exist, which can be further used to design multiple topological interface states.

Then we combine the hyperuniform pillared structures SS* and S*S and construct the SSH-like model SS*S*S. As the topological interface states are localized in the middle of the combined structures rather than the edges, they can exist independently of the outermost boundary conditions. We first regard the combined structure SS*S*S as a supercell and apply periodic boundary conditions to calculate its band structure, as shown in Fig. 5(a). One can see that there are two new red bands in each nontrivial bandgap [indicated by the light gray region in Fig. 4(d)], which are the topological interface bands. The reason for the two interface branches is that in the super-periodic structure, each supercell contains two interfaces, namely, the interfaces in the middle and both ends. In addition, the small dispersion (deviation from flatness) of the interface branches results from the finite size of the supercell, which does not sufficiently isolate the consecutive interfaces in the neighboring supercells, especially in narrow bandgaps where the interface modes are more extended. To isolate the consecutive interfaces, each subsystem in the supercell needs to have a larger extension. On the contrary, there is no new band appearing in the trivial bandgaps. In addition, in a finite structure with open boundary conditions, the topological interface modes still exist due to their localized character at the interface. To illustrate this, we further calculate the eigenfrequencies of one supercell SS*S*S with free boundary conditions at both ends, and the results are shown as the green and yellow dots in Fig. 5(a). It is found that there is an eigenmode corresponding to the red topological interface bands within each nontrivial bandgap marked by a yellow dot.

The distributions of the five topological interface eigenmodes M_1–M_5 indicated by yellow dots are shown in Fig. 5(b), where the color scale represents the amplitude of the total displacement. One can see that most of the energy is localized near the interfaces indicated by the black dashed line, which also demonstrates

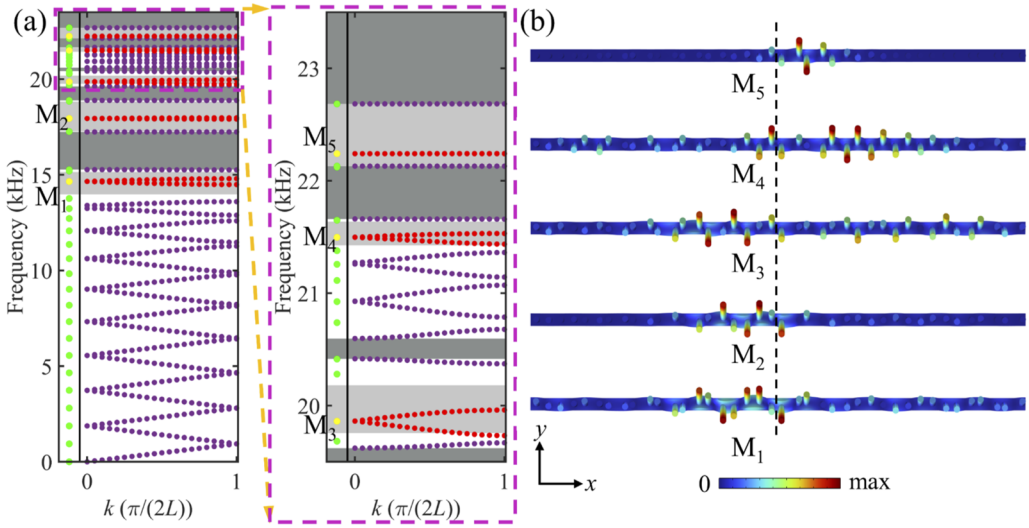

FIG. 5. (a) Band structures of the metabeam constituted by the combined supercell SS*S*S with $\chi = 0.4$ and the eigenfrequencies of one supercell SS*S*S with free boundary conditions at both ends (shown as green and yellow dots). The enlarged view of the high-frequency range is given in the magenta dashed box. The light and dark gray regions represent the nontrivial and trivial bandgaps, respectively. The red bands represent the topological interface bands. The five topological interface states M_1–M_5 of one supercell SS*S*S, indicated by yellow dots, are shown in (b). The black dashed line in (b) indicates the interfaces of the SS* and S*S structures.

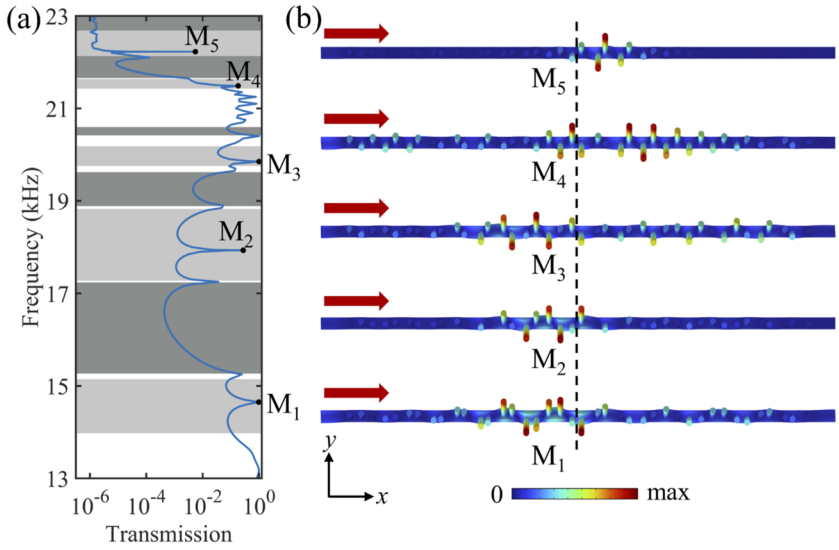

FIG. 6. (a) Transmission spectra of the combined structure SS*S*S with $\chi = 0.4$. The light and dark gray regions represent the nontrivial and trivial bandgaps, respectively. The displacement fields of M_1–M_5 are given in (b). The red arrows indicate the incident waves. The black dashed line in (b) indicates the interfaces of the SS* and S*S structures.

the topological interface modes in analogy to the SSH model. Moreover, the displacements of mode M_5 are strongly localized near the interface. These results also demonstrate that one supercell of the combined metabeam SS*S*S can produce topological interface modes as well.

Furthermore, we calculate the transmission spectra through one supercell of the combined structure SS*S*S, as shown in Fig. 6(a). The transmission model consists of 40 pairs of pillars, which are located according to the SS*S*S distribution with $\chi = 0.4$, and port boundary conditions are applied at both ends to simulate the incoming and outgoing waves. The transmission is large in the passband frequency range (white region) and small in the bandgap frequency range (gray region), as expected. There is a transmission peak in each nontrivial bandgap, as indicated by the black dot, which represents the topological interface mode. The total displacement fields of transmission peaks M_1–M_5 under the left incoming waves are shown in Fig. 6(b). One can see that the displacements are localized near the interface indicated by the black dashed line, and the displacement distributions are very similar to those in Fig. 5(b), which further illustrates the topological interface modes.

C. Hyperuniform metabeam with $\chi = 0.2$

Now we investigate the properties of hyperuniform pillared metabeams with $\chi = 0.2$, which means increasing the level of disorder. Pillar positions for hyperuniform supercell SS* and its SSH-like counterpart S*S are shown in Figs. 7(a) and 7(b), respectively. The band structures of the metabeams with the supercell SS* or S*S are shown in Fig. 7(c). More bandgaps occur below the main bandgap as compared to the results for $\chi = 0.4$, originating from the stronger scattering by the more disordered pillars' distribution in the supercell, which is indicated by the decrease in the zero structure factor in Fig. 2(c). Therefore, a strongly disordered distribution is conducive

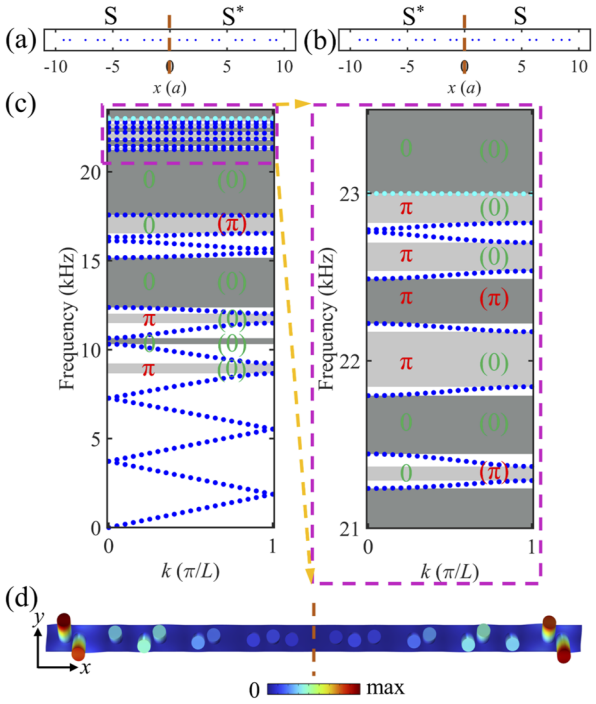

FIG. 7. Pillar positions for $\chi = 0.2$ hyperuniform supercell SS* (a) and its SSH-like counterpart S*S (b). The orange dashed lines indicate the mirror planes separating S and S*. (c) Band structures of the metabeam with the supercells SS* (a) and S*S (b) in the hyperuniform case. The enlarged view of the high-frequency range is given in the magenta dashed box. The left and right values represent the Zak phases of bandgaps in the metabeam SS* (a) and S*S (b), respectively. The light and dark gray regions represent the nontrivial and trivial bandgaps, respectively. The mode of the cyan band at $k = 0$ in panel (c) is given in (d).

to opening bandgaps at low frequencies. However, their widths remain small. Similar to the bands for $\chi = 0.4$, the 20th band marked by cyan near the main bandgap is flat, and the distribution of the displacement mode at $k = 0$ is given in Fig. 7(d). One can see that in the considered structure, vibrations are mostly localized near the two edges, which is different from Figs. 4(e) and 4(f).

The Zak phases of bandgaps for hyperuniform metabeam with supercells SS* and S*S are labeled on the left and right in Fig. 7(c), respectively. The nontrivial bandgaps with different Zak phases and the trivial bandgaps with the same Zak phases are, respectively, indicated by the light and dark gray regions. In this case, more nontrivial bandgaps appear, and a few nontrivial bandgaps exist at lower frequencies. In addition, there are two wide trivial bandgaps in this model, which would be beneficial for broadband low-frequency wave attenuation.

The band structures of the metabeam for SSH-like combined supercell SS*S*S corresponding to $\chi = 0.2$ are shown in Fig. 8(a), in which red bands represent the topological interface bands. It is noticed that the first four red bands are relatively dispersive rather than flat, which means the topological states are weakly localized and relatively penetrating into the bulk parts. The eigenfrequencies of one combined supercell SS*S*S with free boundary conditions at both ends are shown as green and yellow dots, where the seven yellow dots labeled P_1–P_7 represent the topological interface modes in the nontrivial bandgaps (indicated by the light gray regions). The transmission spectra of the metabeam with one combined supercell SS*S*S with $\chi = 0.2$ are calculated and shown in Fig. 8(b), where the transmission peaks in light gray regions represent the seven topological interface modes P_1–P_7. It is worth noting that the quality factors of the first two topological interface modes, P_1 and P_2, are low, which is related to the narrow bandgaps, dispersive bands, and expanding states. Furthermore, the transmissions in the two wide trivial bandgaps are small, which can be utilized for broadband wave attenuation.

D. Robustness of topological states

Finally, we examine the robustness of the topological modes by introducing randomness in the pillars' positions in two ways: maximum position perturbation δ_x along the x-axis (while keeping the xOz symmetry plane) and δ_y along the y-axis (without the xOz symmetry plane). For the sake of simplicity, we assume that any pair of upper and lower pillars with central symmetry moves simultaneously. We chose the first topological mode M_1 for $\chi = 0.4$ and the second topological mode P_2 for $\chi = 0.2$ to show the influences of the pillar's position perturbation on the transmission, and the results are given in Fig. 9. We show the effect of δ_x in Figs. 9(a) and 9(b), where one can notice that the transmission curves have almost no change for 1 and 2 mm perturbations, except for a small peak frequency shift of less than 0.3% for $\chi = 0.4$ and 0.2, respectively. The transmission curves start to change significantly for a 3 mm perturbation, including a reduction and blueshift of the peak amplitude while remaining below 1.5%. For the influences of δ_y shown in Figs. 9(c) and 9(d), the transmission peaks gradually redshift with the increasing perturbation strength δ_y for both hyperuniform metabeams, where the shifts under 1 and 2 mm perturbations are small and become larger under 3 mm perturbations. In addition, the transmission peak amplitudes for 2 mm perturbations decrease slightly, while those for 3 mm perturbations decrease significantly. However, it is observed that the transmission shapes are always conserved for any of the considered perturbations, and, in particular, the topological states remain inside

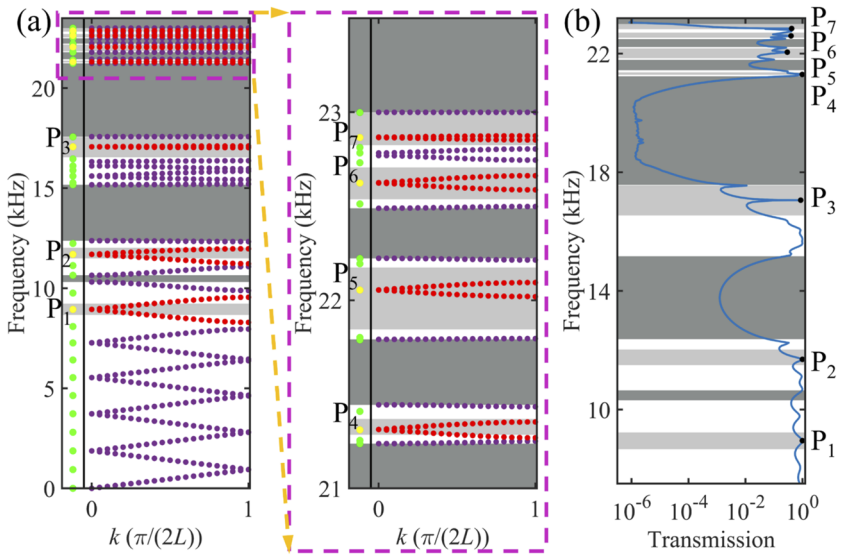

FIG. 8. (a) Band structures of the metabeam constituted by the combined supercell SS*S*S with $\chi = 0.2$ and the eigenfrequencies of one supercell SS*S*S with free boundary conditions at both ends (shown as green and yellow dots). The enlarged view of the high-frequency range is given in the magenta dashed box. The light and dark gray regions represent the nontrivial and trivial bandgaps, respectively. The red bands represent the topological interface bands. The seven topological interface states of one supercell, SS*S*S, indicated in yellow are marked as P_1–P_7. (b) Transmission spectra of the combined structure SS*S*S with $\chi = 0.2$.

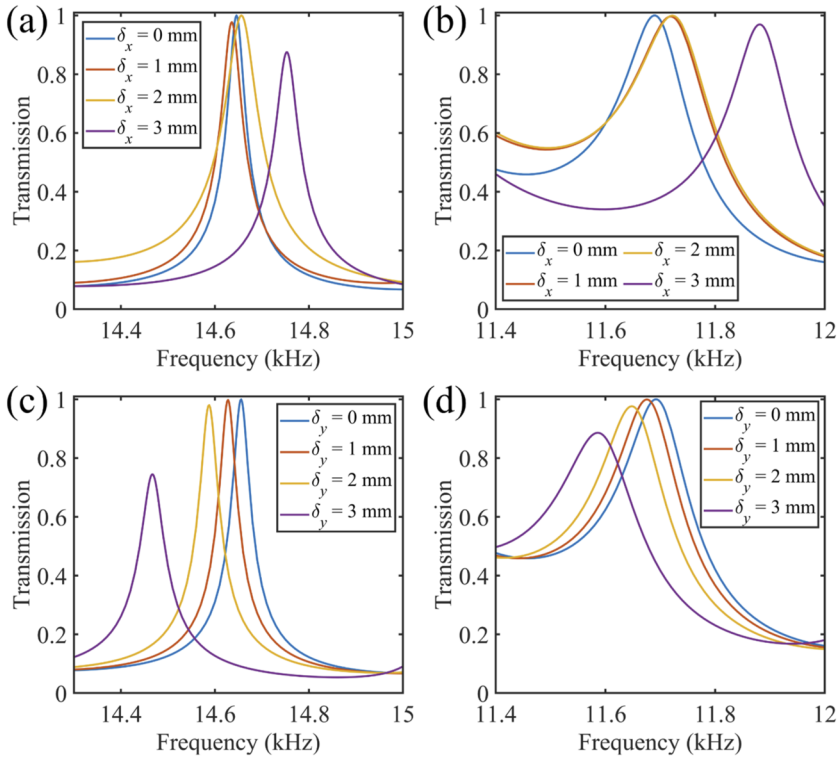

FIG. 9. Robustness of the topological transmission peaks against the pillar's position perturbation along the x direction with the random degree δ_x for the $\chi = 0.4$ (a) and $\chi = 0.2$ (b) combined metabeams, and along the y direction with the random degree δ_y for the $\chi = 0.4$ (c) and $\chi = 0.2$ (d) combined metabeams.

the bandgap range. Thus, the results can demonstrate that the topological modes have a certain robustness to external disturbances. In addition, immunity to perturbations is better satisfied when the symmetry of the structure is conserved (as for δ_x) than when it is broken (as for δ_y).

Furthermore, we investigate the influences of stealthiness parameters χ on the main bandgaps. The results show that the central frequency and width of the main bandgap decrease with decreasing χ values (see the supplementary material, Sec. III).

IV. CONCLUSIONS

In summary, we presented the multiple topological interface modes in SSH-like hyperuniform metabeams. The metabeams consist of pillars symmetrically positioned on the upper and lower surfaces of the host beam, with hyperuniform distribution along the x direction and a mirror symmetry plane. We showed that the hyperuniform metabeam could open new bandgaps at low frequencies, including nontrivial and trivial bandgaps, and have localized modes near the main bandgap, which expands the research scope of traditional metamaterials and phononic crystals and provides more freedom to design various passbands and bandgaps. Furthermore, the SSH-like model is constructed by combining the two hyperuniform metabeams, which have an inverted left half and right half. We demonstrated that multiple topological interface modes occur in the nontrivial bandgaps based on several arguments, such as the Zak phases of the band structures, eigenmodes of finite metabeams, and transmissions. Moreover, we found that the hyperuniform metabeam with lower stealthy parameters χ (namely, more disorder) could open more bandgaps at low frequencies and support more topological interface modes. The bandgaps at low frequencies of hyperuniform structures also have great potential for wave attenuation. Finally, the robustness of the topologically modes is verified by introducing perturbations in the pillars' positions along the x and y directions. The proposed multiple topologically localized states can make up for the shortcomings of the single operating frequency of the traditional single topological localized state and improve the efficiency of potential applications such as energy harvesting and sensing. Our work presents a versatile platform for studying disordered hyperuniform metamaterials and topological properties and may open promising avenues for broadband wave attenuation, energy localization, sensing, and robust transport.

SUPPLEMENTARY MATERIAL

See the supplementary material for the specific positions of the points of the hyperuniform configuration used in the study, the topological states for all types of waves in the hyperuniform metabeams, and the variation of the main bandgap with χ-values for antisymmetric shear waves.

ACKNOWLEDGMENTS

This work was supported by the National Natural Science Foundation of China (Grant Nos.12272267 and 52278411), the Young Elite Scientists Sponsorship Program by CAST (Grant No. 2021QNRC001), the Shanghai Science and Technology Commission (Grant Nos. 22JC1404100 and 21JC1405600), the Special Funds of the Tongji University for "Sino-German Cooperation 2.0 Strategy," and the Fundamental Research Funds for the Central Universities. The first author is grateful for the support of the China Scholarship Council (Grant No. 202206260205). This work was part of the project MAGNIFIC, which has received funding from the European Union's Horizon Europe research and innovation program under Grant Agreement No. 101091968. The project is also supported by the French national research agency ANR under Grant Agreement No. ANR-19-CE24-0014.

AUTHOR DECLARATIONS

Conflict of Interest

The authors have no conflicts to disclose.

Author Contributions

Runcheng Cai: Data curation (equal); Formal analysis (equal); Investigation (equal); Methodology (equal); Software (equal); Validation (equal); Visualization (equal); Writing – original draft (equal); Writing – review & editing (equal). **Yan Pennec**: Conceptualization (equal); Formal analysis (equal); Funding acquisition (equal); Methodology (equal); Project administration (equal); Resources (equal); Supervision (equal); Writing – original draft (equal); Writing – review & editing (equal). **Laurent Carpentier**: Methodology (equal); Software (equal); Writing – original draft (equal); Writing – review & editing (equal). **Yabin Jin**: Conceptualization (equal); Funding acquisition (equal); Methodology (equal); Project administration (equal); Resources (equal); Supervision (equal); Validation (equal); Writing – original draft (equal); Writing – review & editing (equal). **Timon Rabczuk**: Methodology (equal); Software (equal); Writing – original draft (equal); Writing – review & editing (equal). **Xiaoying Zhuang**: Conceptualization (equal); Funding acquisition (equal); Methodology (equal); Project administration (equal); Resources (equal); Supervision (equal); Writing – original draft (equal); Writing – review & editing (equal). **Bahram Djafari-Rouhani**: Conceptualization (equal); Funding acquisition (equal); Methodology (equal); Project administration (equal); Resources (equal); Supervision (equal); Validation (equal); Writing – original draft (equal); Writing – review & editing (equal).

DATA AVAILABILITY

The data that support the findings of this study are available from the corresponding authors upon reasonable request.

REFERENCES

[1] P. A. Deymier, *Acoustic Metamaterials and Phononic Crystals* (Springer Science & Business Media, 2013).
[2] M.-H. Lu, L. Feng, and Y.-F. Chen, "Phononic crystals and acoustic metamaterials," Mater. Today **12**, 34–42 (2009).
[3] L. He, H. Guo, Y. Jin, X. Zhuang, T. Rabczuk, and Y. Li, "Machine-learning-driven on-demand design of phononic beams," Sci. China-Phys. Mech. Astron. **65**, 214612 (2022).
[4] Y. Jin, B. Djafari-Rouhani, and D. Torrent, "Gradient index phononic crystals and metamaterials," Nanophotonics **8**, 685–701 (2019).
[5] S. A. Cummer, J. Christensen, and A. Alù, "Controlling sound with acoustic metamaterials," Nat. Rev. Mater. **1**, 16001 (2016).
[6] G. Ma and P. Sheng, "Acoustic metamaterials: From local resonances to broad horizons," Sci. Adv. **2**, e1501595 (2016).
[7] Y. Jin, R. Kumar, O. Poncelet, O. Mondain-Monval, and T. Brunet, "Flat acoustics with soft gradient-index metasurfaces," Nat. Commun. **10**, 143 (2019).
[8] H. Xue, Y. Yang, and B. Zhang, "Topological acoustics," Nat. Rev. Mater. **7**, 974–990 (2022).
[9] M. Xiao, G. Ma, Z. Yang, P. Sheng, Z. Zhang, and C. T. Chan, "Geometric phase and band inversion in periodic acoustic systems," Nat. Phys. **11**, 240–244 (2015).
[10] S. H. Mousavi, A. B. Khanikaev, and Z. Wang, "Topologically protected elastic waves in phononic metamaterials," Nat. Commun. **6**, 8682 (2015).
[11] Z.-D. Zhang, S.-Y. Yu, H. Ge, J.-Q. Wang, H.-F. Wang, K.-F. Liu, T. Wu, C. He, M.-H. Lu, and Y.-F. Chen, "Topological surface acoustic waves," Phys. Rev. Appl. **16**, 044008 (2021).
[12] Z.-w. Li, X.-s. Fang, B. Liang, Y. Li, and J.-c. Cheng, "Topological interface states in the low-frequency band gap of one-dimensional phononic crystals," Phys. Rev. Appl. **14**, 054028 (2020).
[13] W. Zhou, W. Zhou, and C. Lim, "Topological edge modeling and localization of protected interface modes in 1D phononic crystals for longitudinal and bending elastic waves," Int. J. Mech. Sci. **159**, 359–372 (2019).
[14] Y. Jin, W. Wang, Z. Wen, D. Torrent, and B. Djafari-Rouhani, "Topological states in twisted pillared phononic plates," Extreme Mech. Lett. **39**, 100777 (2020).
[15] Z. Gu, H. Gao, T. Liu, S. Liang, S. An, Y. Li, and J. Zhu, "Topologically protected exceptional point with local non-Hermitian modulation in an acoustic crystal," Phys. Rev. Appl. **15**, 014025 (2021).
[16] F. Zangeneh-Nejad and R. Fleury, "Topological Fano resonances," Phys. Rev. Lett. **122**, 014301 (2019).
[17] W. Wang, Y. Jin, W. Wang, B. Bonello, B. Djafari-Rouhani, and R. Fleury, "Robust Fano resonance in a topological mechanical beam," Phys. Rev. B **101**, 024101 (2020).
[18] W.-P. Su, J. R. Schrieffer, and A. J. Heeger, "Solitons in polyacetylene," Phys. Rev. Lett. **42**, 1698 (1979).
[19] L. Thatcher, P. Fairfield, L. Merlo-Ramírez, and J. M. Merlo, "Experimental observation of topological phase transitions in a mechanical 1D-SSH model," Phys. Scr. **97**, 035702 (2022).
[20] N. Kaina and R. Fleury, "Hermitian formulation of multiple scattering induced topological phases in metamaterial crystals," Phys. Rev. B **102**, 134303 (2020).
[21] G. J. Chaplain, J. M. De Ponti, G. Aguzzi, A. Colombi, and R. V. Craster, "Topological rainbow trapping for elastic energy harvesting in graded Su–Schrieffer–Heeger systems," Phys. Rev. Appl. **14**, 054035 (2020).
[22] M. Esmann, F. R. Lamberti, P. Senellart, I. Favero, O. Krebs, L. Lanco, C. Gomez Carbonell, A. Lemaître, and N. D. Lanzillotti-Kimura, "Topological nanophononic states by band inversion," Phys. Rev. B **97**, 155422 (2018).
[23] R. El-Ganainy, K. G. Makris, M. Khajavikhan, Z. H. Musslimani, S. Rotter, and D. N. Christodoulides, "Non-Hermitian physics and PT symmetry," Nat. Phys. **14**, 11–19 (2018).
[24] R. Cai, Y. Jin, Y. Li, J. Zhu, H. Zhu, T. Rabczuk, and X. Zhuang, "Absorption-lasing effects and exceptional points in parity-time symmetric non-Hermitian metaplates," J. Sound Vib. **555**, 117710 (2023).
[25] R. Cai, Y. Jin, Y. Li, T. Rabczuk, Y. Pennec, B. Djafari-Rouhani, and X. Zhuang, "Exceptional points and skin modes in non-Hermitian metabeams," Phys. Rev. Appl. **18**, 014067 (2022).
[26] H. Fan, H. Gao, S. An, Z. Gu, S. Liang, Y. Zheng, and T. Liu, "Hermitian and non-Hermitian topological edge states in one-dimensional perturbative elastic metamaterials," Mech. Syst. Signal Process. **169**, 108774 (2022).
[27] Y. Jin, W. Zhong, R. Cai, X. Zhuang, Y. Pennec, and B. Djafari-Rouhani, "Non-Hermitian skin effect in a phononic beam based on piezoelectric feedback control," Appl. Phys. Lett. **121**, 022202 (2022).

[28]W. Zhong, R. Cai, X. Zhuang, T. Rabczuk, Y. Pennec, B. Djafari-Rouhani, and Y. Jin, "Reconfigurable localized effects in non-Hermitian phononic plate," Appl. Phys. Lett. **122**, 222203 (2023).
[29]X. Zhang, T. Zhang, M.-H. Lu, and Y.-F. Chen, "A review on non-Hermitian skin effect," Adv. Phys.: X **7**, 2109431 (2022).
[30]S. Torquato and F. H. Stillinger, "Local density fluctuations, hyperuniformity, and order metrics," Phys. Rev. E **68**, 041113 (2003).
[31]C. E. Zachary and S. Torquato, "Hyperuniformity in point patterns and two-phase random heterogeneous media," J. Stat. Mech.: Theory Exp. **2009**, P12015.
[32]S. Torquato, G. Zhang, and F. H. Stillinger, "Ensemble theory for stealthy hyperuniform disordered ground states," Phys. Rev. X **5**, 021020 (2015).
[33]S. Torquato, "Hyperuniform states of matter," Phys. Rep. **745**, 1–95 (2018).
[34]S. Kuznetsova, J.-P. Groby, L. García-Raffi, and V. Romero-García, "Localized interface modes in one-dimensional hyperuniform acoustic materials," J. Phys. D: Appl. Phys. **54**, 315303 (2021).
[35]R. D. Batten, F. H. Stillinger, and S. Torquato, "Classical disordered ground states: Super-ideal gases and stealth and equi-luminous materials," J. Appl. Phys. **104**, 033504 (2008).
[36]V. Romero-García, N. Lamothe, G. Theocharis, O. Richoux, and L. M. Garcia-Raffi, "Stealth acoustic materials," Phys. Rev. Appl. **11**, 054076 (2019).
[37]É. Chéron, S. Félix, J.-P. Groby, V. Pagneux, and V. Romero-García, "Wave transport in stealth hyperuniform materials: The diffusive regime and beyond," Appl. Phys. Lett. **121**, 061702 (2022).
[38]G. J. Aubry, L. S. Froufe-Pérez, U. Kuhl, O. Legrand, F. Scheffold, and F. Mortessagne, "Experimental tuning of transport regimes in hyperuniform disordered photonic materials," Phys. Rev. Lett. **125**, 127402 (2020).
[39]L. S. Froufe-Pérez, M. Engel, P. F. Damasceno, N. Muller, J. Haberko, S. C. Glotzer, and F. Scheffold, "Role of short-range order and hyperuniformity in the formation of band gaps in disordered photonic materials," Phys. Rev. Lett. **117**, 053902 (2016).
[40]G. Gkantzounis, T. Amoah, and M. Florescu, "Hyperuniform disordered phononic structures," Phys. Rev. B **95**, 094120 (2017).
[41]W. Man, M. Florescu, E. P. Williamson, Y. He, S. R. Hashemizad, B. Y. Leung, D. R. Liner, S. Torquato, P. M. Chaikin, and P. J. Steinhardt, "Isotropic band gaps and freeform waveguides observed in hyperuniform disordered photonic solids," Proc. Natl. Acad. Sci. U. S. A. **110**, 15886–15891 (2013).
[42]T. Amoah and M. Florescu, "High-Q optical cavities in hyperuniform disordered materials," Phys. Rev. B **91**, 020201 (2015).
[43]W. Zhou, Y. Tong, X. Sun, and H. K. Tsang, "Hyperuniform disordered photonic bandgap polarizers," J. Appl. Phys. **126**, 113106 (2019).
[44]H. Tang, Z. Hao, Y. Liu, Y. Tian, H. Niu, and J. Zang, "Soft and disordered hyperuniform elastic metamaterials for highly efficient vibration concentration," Natl. Sci. Rev. **9**, nwab133 (2022).
[45]H. Zhang, H. Chu, H. Giddens, W. Wu, and Y. Hao, "Experimental demonstration of Luneburg lens based on hyperuniform disordered media," Appl. Phys. Lett. **114**, 053507 (2019).
[46]N. P. Mitchell, L. M. Nash, D. Hexner, A. M. Turner, and W. T. Irvine, "Amorphous topological insulators constructed from random point sets," Nat. Phys. **14**, 380–385 (2018).
[47]V. Romero-García, É. Chéron, S. Kuznetsova, J.-P. Groby, S. Félix, V. Pagneux, and L. Garcia-Raffi, "Wave transport in 1D stealthy hyperuniform phononic materials made of non-resonant and resonant scatterers," APL Mater. **9**, 101101 (2021).
[48]O. U. Uche, F. H. Stillinger, and S. Torquato, "Constraints on collective density variables: Two dimensions," Phys. Rev. E **70**, 046122 (2004).
[49]M. Xiao, Z. Zhang, and C. T. Chan, "Surface impedance and bulk band geometric phases in one-dimensional systems," Phys. Rev. X **4**, 021017 (2014).